Supplementary Data

S1. Material

For TSSA fabrication, TPU filament (NinjaTek, USA) was used. TPU sustains very large elastic strains (more than 600%) and returns to its original configuration without permanent set, behavior characteristic of hyperelastic materials and warranting constitutive modeling beyond linear elasticity. The strain-energy density W is represented in terms of the principal invariants I_1, I_2, I_3 of the deformation, as introduced in Equation (S1) and computed from the principal stretches $\lambda_1, \lambda_2, \lambda_3$ (Equations (S2)–(S5)). Candidate hyperelastic forms evaluated for TPU included Neo-Hookean, Mooney–Rivlin, Yeoh, Ogden, and Arruda–Boyce, each distinguished by its specific polynomial or spectral expansion of $W(I_1, I_2, I_3)$ (Table S1)

$$W = W(I_1, I_2, I_3) \tag{S1}$$

$$\lambda = \frac{L}{Lo} = 1 + \epsilon_E \tag{S2}$$

$$I_1 = \sum_{i=1}^{3} \lambda_i^2 \tag{S3}$$

$$I_2 = \sum_{i=1}^{3} \lambda_i^2 \lambda_j^2 \tag{S4}$$

$$I_3 = \lambda_1^2 \lambda_{21}^2 \lambda_3^2 \tag{S5}$$

Uniaxial tensile tests were performed on ASTM D638 dog-bone specimens (Figure S1b) printed under the same process conditions used for the actuators to ensure property transferability. Testing employed an Instron 4202 with a crosshead speed of 100 mm/min, reaching approximately 660% strain at ambient conditions (Figure S1a). The resulting stress–strain data (Figure S2) were imported into ANSYS 2022, which provides curve-fitting utilities for multiple hyperelastic models. Among the candidates listed in Table S1, the five-parameter Mooney–Rivlin variant provided the most accurate and stable reproduction of the TPU-85 response (Figure S2). Because elastomeric TPUs typically exhibit negligible volumetric change under quasi-static loading, the material was treated as incompressible within the fitting procedure, consistent with the parameterization used in subsequent simulations.

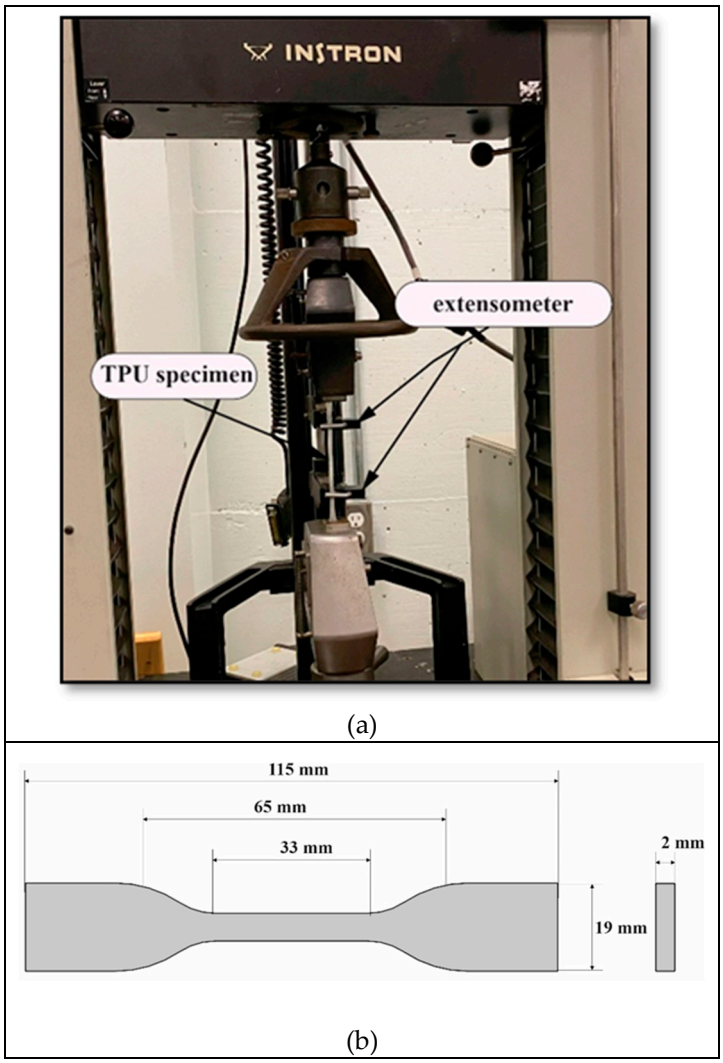


Figure S1. (a) Tensile test experimental setup (b) specimen design

Table S1. Hyperelastic models and their corresponding strain energy functions.

Hyperelastic Model	Incompressible Strain Energy Function
Mooney-Rivlin	$W=\sum_{i=1}^{2} C_i \ \ (I_i - 3)$
Yeoh	$W=\sum_{i=1}^{3} C_i \ \ (I_1 - 3)^i$
Ogden	$W = \sum_{i=1}^{N} \frac{\mu i}{\alpha i} (\lambda_1^{\alpha i} + \lambda_2^{\alpha i} + \lambda_3^{\alpha i} - 3)$
Neo-Hookean	$W=C_{10}(I_1-3)$

The ANSYS curve-fitting workflow was used to identify model constants directly from the experimental dataset. For the five-parameter Mooney–Rivlin model adopted here, the strain-energy density expands as in Equation (S6), with coefficients $(C_{10}, C_{01}, C_{20}, C_{11}, C_{02})$obtained by regression. The identified constants for TPU-85 are listed in Table S2 (units: MPa):
$C_{10} = -3.1992,\ C_{01} = 6.977,\ C_{20} = 0.0281,\ C_{11} = -0.074972,\ C_{02} = 0.92155$; the incompressibility parameter is $D_1 = 0$. These values capture the compliant initial response and the pronounced strain-hardening at large stretch observed experimentally, and they are

suitable for finite-element analyses of thin-wall folds and hinge-like regions in the TSSA. to:

$$W = C_{10}(I_1 - 3) + C_{01}(I_2 - 3) + C_{11}(I_1 - 3)(I_2 - 3) + C_{10}(I_1 - 3) + C_{20}(I_1 - 3)^2 + C_{02}(I_1 - 3)^2 \quad \text{(S6)}$$

Table S2. Lists the hyperelastic material constants identified for TPU 85using the Mooney-Rivlin 5-parameter model.

Parameters	Value (MPa)
C10	-3.1992
C01	6.977
C20	0.0281
C11	-0.074972
C02	0.92155
Incompressible parameter D1	0

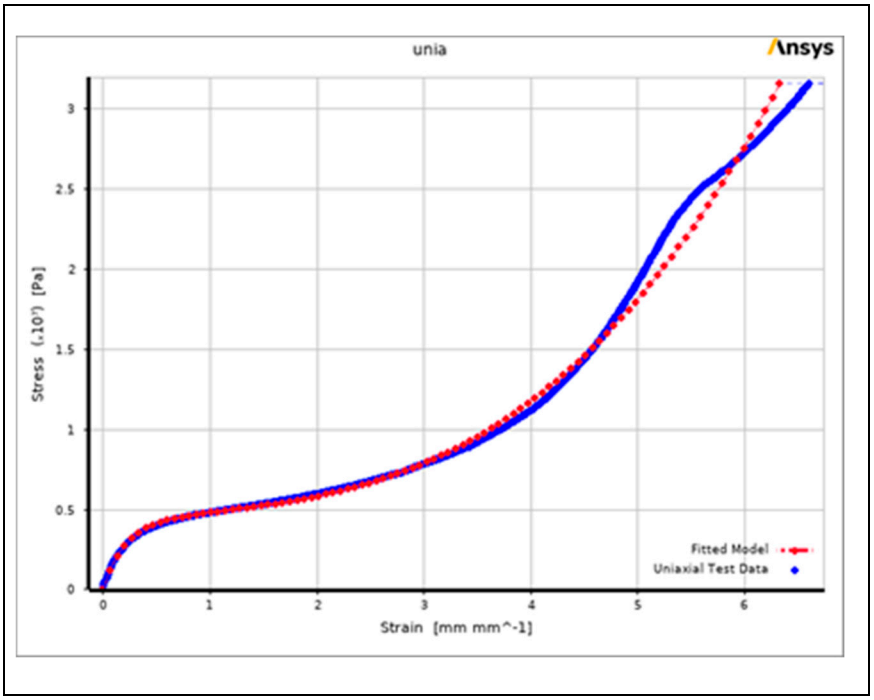


Figure S2. Curve fitting of TPU 85 material using Mooney Rivlin's 5-parameter mate-rial model

S2. Integration with Complementary Sleeve Actuators

The Twisting Soft Sleeve Actuator (TSSA) integrates with a Linear Sleeve Actuator (Linear SLA) and a Bending Sleeve Actuator (Bending SLA) to provide combined twist–bend–translate motion in a compact, wearable form. Shared thin-wall, low-volume construction and an adjustable inner radius enable axis co-alignment with the target joint for efficient force transmission. A practical layout places a Bending SLA concentrically between two TSSAs of opposite helical handedness, yielding bidirectional torsion with in-plane bending (Figure S3). Independent pressure channels decouple the degrees of freedom, and stabilization layers limit radial growth to reduce cross-talk. This modular stack supports soft wrists, elbow orthoses, and continuum segments requiring coordinated multi-DoF control.

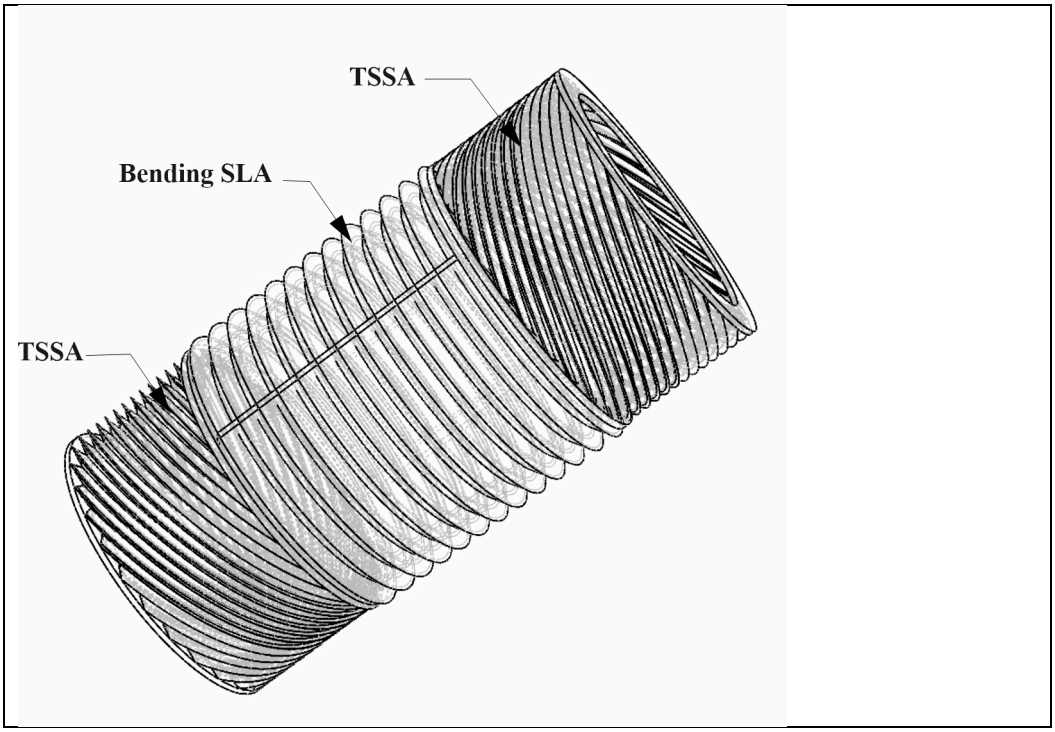


Figure S3. Conceptual integration of TSSA with Bending SLA.